An Automatic Method for Counting Annual Rings in Noisy Sawmill Images

Kristin Norell

Centre for Image Analysis, Swedish University of Agricultural Sciences
kristin@cb.uu.se

Abstract. The annual ring pattern of a log end face is related to the quality of the wood. We propose a method for computing the number of annual rings on a log end face depicted in sawmill production. The method is based on the grey-weighted polar distance transform and registration of detected rings from two different directions. The method is developed and evaluated on noisy images captured in on-line sawmill production at a Swedish sawmill during 2008, using an industrial colour camera. We have also evaluated the method using synthetic data with different ring widths, ring eccentricity, and noise levels.

1 Introduction

When sawing wood, the quality of the resulting product is related to the quality of the timber. The timber quality influences the price to wood suppliers as well as the usage. One parameter that is related to wood quality is the annual ring width, which is used at Swedish sawmills as a parameter for classification of the timber into different quality classes. The estimation of the annual ring width is made by visual inspection by a log scaler as the timber passes on a conveyor belt. An automatic system based on image analysis of timber end faces would reduce the work load for the log scaler and has the possibility to be more consistent and thus preferable over visual inspection.

The problem of measuring annual ring width using image analysis has been addressed before. The task has often been to measure the ring width for a dendrochronology application or to measure the amount of earlywood and latewood. In such cases, high resolution images depicting end faces with high readability are needed. Semi-automatic methods based on edge detection in high resolution microscopic images are presented in [1] and [2], as well as in [3] and [4], where sanded end faces are depicted using a scanner with 600 dpi resolution. The methods suggested in the mentioned papers are not applicable to our problem, as the quality of images that can be captured in an operating sawmill is much worse.

In [5] the images are captured in the field using a digital camera. Their method uses edge detection to find pixels that belong to the annual rings and fits polygons to the detected edges. The starting position for the polygon is the outer boundary of the end face and the polygon is then shrunken to detect the rings. In the trees considered here the annual rings are usually much narrower than in the example images shown in [5]. With only a few pixels separating each annual ring in combination with the images being noisy, this method is not applicable.

P. Foggia, C. Sansone, and M. Vento (Eds.): ICIAP 2009, LNCS 5716, pp. 307–316, 2009.

In [6] the annual rings are counted using the Fourier transform in a local region. The distance from the centre of the Fourier spectra to the maximum corresponds to the number of rings in the region. The number of annual rings along a path perpendicular to the annual ring pattern is computed by taking the Fourier transform of a number of pixels along the path and combining the results. A problem with this method is that only the dominating frequency influences the result. If the tree has been growing fast for one year, e.g., due to felling of surrounding trees, or slow due to a dry spring, this will not be visible in the spectrum. The resolution is also a problem in our case, since if the local region does not include more than about three rings, the maximum in the Fourier spectra will be difficult to distinguish from the high DC-component in the centre of the spectra.

We present an automatic method to compute the number of annual rings in end faces depicted in sawmill environment. Images of Scots pine are captured in on-line production at a sawmill, where all end faces are sawn with harvester or chain saw, stored in the forest for some time and then transported with truck to the sawmill. We compute the number of rings in images where the annual rings can be counted by visual inspection, as well as in synthetic images of different ring width and noise levels.

2 Data

End face images used in the development and evaluation of the method are captured at Setra Nyby sawmill in Sweden. The images are captured automatically at the sawmill measurement station while the logs pass on a conveyor belt with a speed of approximately 1.1 m/s. The camera is placed above the conveyor belt and captures images as the logs move away from the camera.

The camera is a colour camera suitable for industrial use, a PixeLINK PL-A782 with a CMOS sensor. A Bayer mosaic [7] pattern is used for capturing colour images. The imaging is performed using a rolling shutter technique, meaning that all pixels are not exposed in parallel, only a few pixel rows at a time. Images are 1800×1536 pixels, and the pixel size in the captured images is approximately 0.4 mm.

The camera is placed at the measurement station so that it is facing the log scaler. Unfortunately this placing means that it is impossible to use a flash in the imaging, since it would be a large disturbance for the log scaler. The rolling shutter technique in combination with a moving end face will therefore give motion blur in the image. The fact that the camera is placed above the conveyor belt means that we have an angle of approximately 20 degrees between the end face and the imaging plane which will create a distortion of the image, compressing it slightly in height. The motion blur and image distortion will result in the fact that each annual ring is more difficult to distinguish where the rings are horizontal, i.e., above and below the pith.

A training set of 24 images and an evaluation set of 20 images are drawn from images of Scots pine captured monthly during 2008. These are images in which the annual rings can be counted by visual inspection at least along some direction, which is not the case for all captured images.

2.1 Synthetic Data

A number of synthetic images were created for evaluation and testing of the proposed method. The synthetic images are based on a sinus signal modelling the annual ring pattern. A circular sinus pattern of frequency f can be created by applying a sinus function to the Euclidean distance from an image origin, $\boldsymbol{p}_0$. To distort the perfectly circular pattern a 2D linear function is added to the distance image before applying the sinus function:

$$S(\boldsymbol{p}) = \sin\left(2\pi f\left(\|\boldsymbol{x}\| + k \cdot \boldsymbol{x}\right)\right), \tag{1}$$

where $\boldsymbol{p}$ is a pixel, $\boldsymbol{x} = \boldsymbol{p} - \boldsymbol{p}_0$ and k determines the slope of the linear function. The higher value of k, the more eccentricity of the rings. Random Gaussian noise with mean value 0 and standard deviation σ_n is added to the sinus pattern. The images are smoothed with a 2D Gaussian filter with standard deviation $\sigma = 2$ and scaled to the intensity range $50 - 115$ to resemble the captured end face images.

3 The Proposed Method

The goal of the method is to count the number of annual rings in correspondence with the instructions from the Swedish Timber Measurement Council. The annual rings should be counted in a region of 2-8 cm from the pith in the direction of the most sparse annual ring pattern. The area around the chosen direction is not permitted to include knots or other disturbances that influence the annual ring pattern [8]. To compute the number of rings in the direction with the most sparse rings, i.e., the lowest number of rings, requires knowledge of the annual ring pattern on the entire end face. At this point we do not attempt to compute the number of rings on the entire end face, but to automatically choose a direction proper for measuring the number of annual rings and compute the number of rings in that area. Such a direction shall have undisturbed annual rings with as high readability as possible. We will only consider annual rings in the area of 2 to 8 cm from the pith in the computations. We denote this area A_{2-8}.

3.1 Outline of the Method

The complete method consists of several steps:

1. Pith detection
2. Detection of proper region, P for measuring
3. Creation of a cost image, I in P
4. Detection of ring pattern in P
5. Computation of the number of rings.

The colour images are converted into grey level images before computations using the standard conversion $Y = 0.2989 \cdot R + 0.5870 \cdot G + 0.1140 \cdot B$ where R, G, and B represent the red, green and blue colour channels, respectively [9]. The signal to noise ratio in the blue channel of the captured images is low, therefore only the red and green channels are considered which is achieved by setting $B = 0$ before conversion.

No segmentation of the end faces is performed. The background in the images is dark, but not completely black, and do not disturb the analysis.

3.2 Pith Detection

The pith can be detected using the method described in [10] where local orientations in the image are detected and combined to estimate the pith position. See [10] for computational details.

3.3 Detection of Proper Region

To detect a suitable region for measurements is to detect a region with as clearly visible ring pattern as possible, without disturbances like knots, dirt, or snow. A clearly visible and undisturbed ring pattern is a region where, locally, the rings are parallel ridges, i.e., a 2D signal varying only in one direction. The direction of variation is ideally the direction towards the pith, i.e., the local orientation of the region is the direction towards the pith.

The local orientation, $\varphi(p)$, is computed for all pixels, p. Here we use the computation of local orientation that is included in the suggested pith detection method [10], with filters described in [11]. The computation of local orientation is fast and can be applied to the image even if another pith detection method is preferred. For each pixel, the angle from the detected pith is also computed and used as a reference, or ground truth, $\varphi_{gt}(p)$.

To detect the best direction for computations the image is divided into N overlapping regions, P_i, covering $4\frac{2\cdot\pi}{N}$ radians each. The regions are limited radially by the distance to the pith, considering only the area A_{2-8}. In each of the regions P_i an error is computed from the sum of the difference between detected local orientation and $\varphi_{gt}(p)$ for all pixels in the region

$$E_i = \sum_{p \in P_i} = |\varphi_{gt}(p) - \varphi(p)|, \tag{2}$$

where E_i is the error for region P_i. The direction D with the smallest error is chosen for further computations

$$D = j \mid E_j = \min_i(E_i), \quad i = 1, 2, \ldots, N. \tag{3}$$

Figure 1 shows the area A_{2-8} for an end face image with $N = 36$ different directions as well as the error, E_i for each region. Here $D = 14$ minimizes the error, giving the region P_{14} which is marked in the image with the limiting directions in white.

Due to the imaging technique giving motion blur and image distortion affecting mostly areas above and below the pith as described in Section 2, these regions are ignored when choosing a proper direction. This can easily be changed if another imaging technique is used.

3.4 Creating Cost Image

A cost image is needed in the further computations in which a clear annual ring pattern is wanted. The original image could be used but it is even better to use a contrast enhanced image. To improve the contrast in the images the method suggested in [12] is used, where local contrast enhancement is performed based on the local maximum,

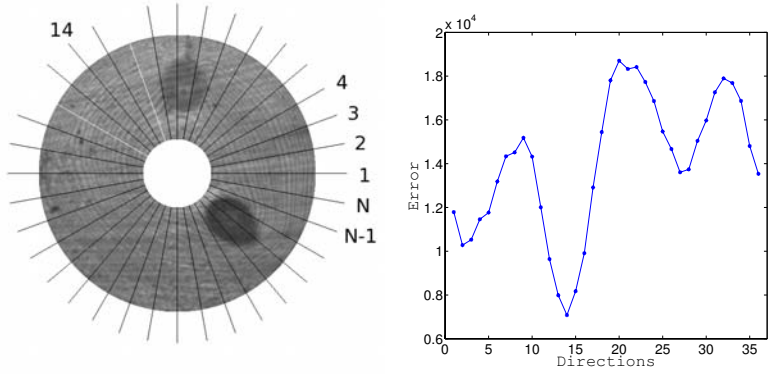

Fig. 1. An end face and the error computed for different regions. The limiting directions of P_{14} are shown as white lines.

minimum and average. The computations are made using a propagation scheme. A conductivity factor, C in the range 0 and 1 is used to determine the size of the propagation window, see [12] for computational details, and the image is enhanced depending on the range of the input image. If the range is smaller than a threshold, ω_0 the signal is considered as noise and the output range is compressed in this area. By visual inspection it was concluded that the suggested noise reduction does not improve the images in our case, thus $\omega_0 = 0$ is used. The parameter $C = 0.85$ has been chosen from experiments using the training data, described in Section 4. The contrast enhancement is computed in region P_D.

3.5 Detection of Annual Ring Pattern

The number of annual rings in region P_D can be estimated by applying the grey-weighted polar distance transform (GWPDT) described in [13]. The GWPDT is an anisotropic distance transform where the polar coordinates (r, θ) of the pixels are considered. By using different costs on propagation in the angular and radial direction, the distance propagates with different speed in the different directions. By setting the weight in the angular direction, ω_θ and the weight in the radial direction, ω_r, so that an angular step has lower cost than the radial, the distance will propagate faster in the angular direction.

We apply the GWPDT from both the directions

$$D_{-2} = D - 2 \mod (N) \tag{4}$$

$$D_{+2} = D + 2 \mod (N) \tag{5}$$

to the region P_D. We let the contrast enhanced image have the range $1 - 50$ and use it as a cost function in the GWPDT with weights $\omega_r = 5/r(p)$ and $\omega_\theta = 1$, where $r(p)$ is the radial coordinate for pixel p.

The cost image with low values in the dark parts of the annual rings together with the GWPDT propagating faster in angular direction than radial will result in fast propagation in dark parts of the annual rings, i.e., we get low distance values in the dark rings.

The two distance images that are the result from applying the GWPDT are analysed along a ray outwards in the direction D. We let S_{D-2} and S_{D+2} denote the one dimensional signals in direction D for GWPDT applied in D_{-2} and D_{+2}, respectively. For S_{D-2} and S_{D+2}, ideally, each local minimum corresponds to the dark part of an annual ring. This is not always the case however, since the images are noisy and annual ring pattern is far from ideal.

In the computations and analysis of the GWPDT we consider the pixels covering a distance of 1 to 9 cm from the pith to be certain to include rings close to the 2 and 8 cm limits.

3.6 Estimation of the Number of Annual Rings

Of the several local minima in S_{D-2} and S_{D+2} many correspond to annual rings, but not all. To count the local minima that correspond to annual rings we combine the result from the two distance transforms by performing elastic registration of the signals. In elastic registration both signals can be stretched or compressed along the signal indexes to best match each other. Here dynamic programming is used for the registration with the same approach as in [14], where the total cost for registration of signals R and S is given by the following:

$$C(R_1^i, S_1^j) = c(R_i, S_j) + \min \begin{cases} C(R_1^i, S_1^{j-1}) + g \\ C(R_1^{i-1}, S_1^{j-1}) \\ C(R_1^{i-1}, S_1^j) + g \end{cases} \tag{6}$$

where $C(R_1^i, S_1^j)$ is the total cost for registering signal R from index 1 to index i with signal S from index 1 to index j, $c(R_i, S_j)$ is the local cost between the signals at index i and j, respectively, and g is a penalty for compressing and stretching the signals. The local cost function

$$c(R_i, S_j) = (R_i - S_j)^2 \tag{7}$$

is used here. The value of the parameter $g = 0.2$ is determined using the training set, see Section 4.

Figure 2(a) shows parts of two signals S_{D-2} and S_{D+2}. Registration is performed to detect local minima, not general intensity, therefore the focus is on the local extrema. For each of the two signals considered, all values that are not local extrema are set to zero. The signals to register are then created by taking the difference between each local extrema and the previous one. The difference signals and registered signals are shown in Figure 2(b) and 2(c), respectively.

3.7 Detection of Rings

After registration, the signals are analyzed for the indexes covering pixels from 2 to 8 cm from the pith. All local minima that are registered to the same index are counted as

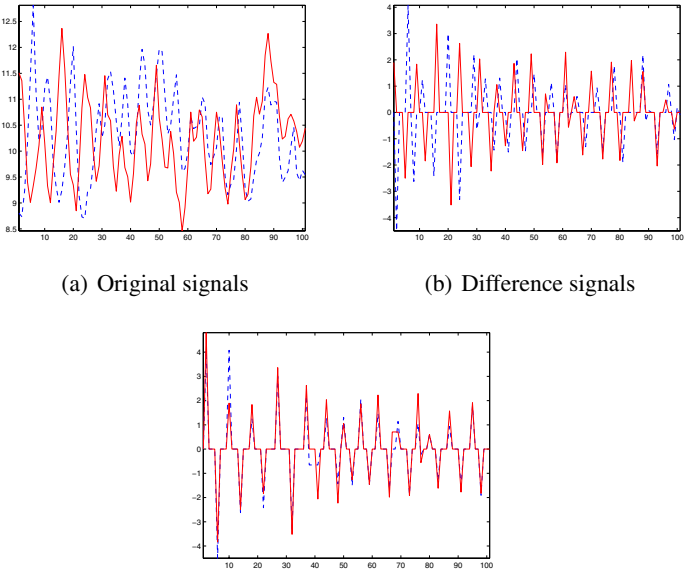

(a) Original signals (b) Difference signals

(c) Registered signals

Fig. 2. Result from the elastic registration

rings. Other local minima are analyzed further: If there exist at least one local minimum in both signals between two registered minima it is counted as an annual ring. The number of extra rings between two registered minima is $\min(k, l)$ where k is the number of local minima in signal S_{D-2} and l is the number of local minima in signal S_{D+2}.

4 Results

The 24 images in the training set have been used to find proper values of the conductivity factor, C in the contrast enhancement and the cost, g in the registration of the signals. The result for different parameters are shown in Figure 3(a). For all combinations of parameters the number of detected rings, M, is compared with the ground truth, M_{gt} and summed, $e = \sum_{n=1}^{24} |M - M_{gt}|$. The ground truth have been established by visual inspection of the images in the automatically chosen directions. The parameters that gave the lowest error were $C = 0.80$ or $C = 0.85$ and $g = 0.2$, thus we have chosen to use $C = 0.85$ and $g = 0.2$ in all computations.

The results from the evaluation set is shown in Figure 3(b). The histogram shows the difference between the counted number of rings and the ground truth, $M - M_{gt}$. We can see that the proposed method underestimates the number of rings slightly.

We have tested the method on the synthetic images described in Section 2.1, using different values of the frequency f, the slope k of the linear function disturbing the circular pattern, and the noise level σ_n. We used $N = 36$ different regions, but computed the number of rings only in every other of them, i.e. in 18 directions. Figure 4(a) shows

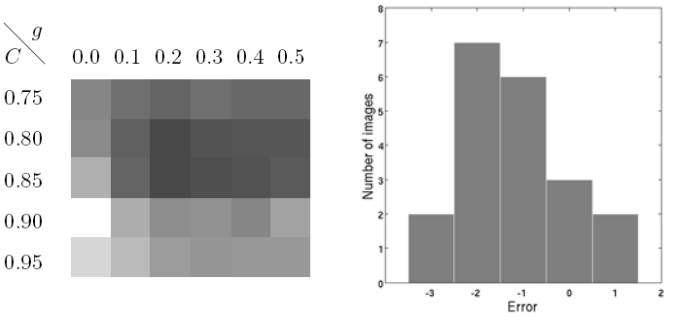

(a) Estimation of parameters from training data.

(b) Result for evaluation data, $M - M_{gt}$

Fig. 3. Parameters computed using training set and results for the evaluation set

the absolute value of the errors summed over all different directions $\sum_{d=1}^{18} |M^d - M_{gt}^d|$, where M^d is the number of detected rings in direction d. The result is shown for five different frequencies and six different values of the parameter k. All images have noise level $\sigma_n = 0.5$. Figure 4(b) shows results for images of frequency $f = 0.17$ with six different values of k and four different noise levels, σ_n. As can be expected high frequency, high noise level and high eccentricity gives considerable errors.

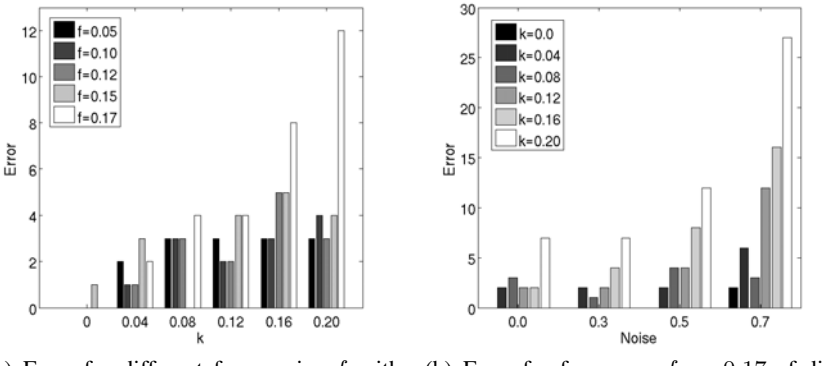

(a) Error for different frequencies f with $k = 0.0 - 0.20$ and $\sigma_n = 0.5$

(b) Error for frequency $f = 0.17$ of different k and different noise levels $\sigma_n = 0.0 - 0.7$.

Fig. 4. Results for synthetic images. Note the different scales on the vertical axis of the two plots.

The result for one of the real images from the evaluation set is shown in Figure 5(a). This is one of the end faces where the number of rings is underestimated by 2. The detected rings are shown as white pixels along the direction in which we computed the number of rings. The positions for the errors, i.e., non-detected annual rings, are marked with white arrows. Figure 5(b) shows the detected rings for a part of the synthetic image

with $f = 0.17$, $k = 0.16$ and $\sigma_n = 0.7$. Detected rings are shown as black pixels. The local minima not registered to the same index are also marked using blue and red pixels for the different signals. The image shows one error which is marked with a white arrow. The positions with non-registered local minima that are correctly counted as rings are marked with black arrows. It can be seen from Figure 4(b) that the total sum of the errors for this image is around 17, i.e., the mean error for each direction is around 1.

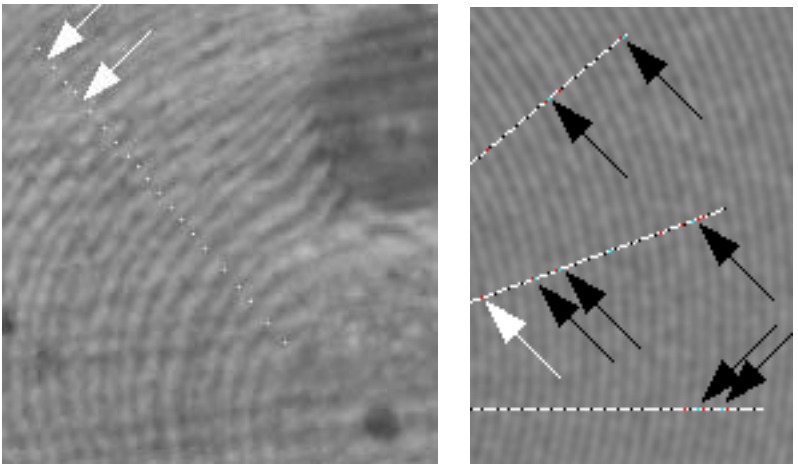

(a) Result shown on a contrast enhanced end face image where $M - M_{gt} = -2$.

(b) Result for a synthetic image with $f = 0.17$, $k = 0.16$, $\sigma_n = 0.7$.

Fig. 5. Example of results for one real and one synthetic image

5 Discussion

We have presented a method for automatic computations of the number of annual rings on end face images from Scots pine, taken in sawmill production. We have computed the number of rings in a training set and evaluation set from on-line captured images, as well as on synthetic data. The method has also been evaluated on synthetic images with different annual ring width, eccentricity and noise level.

In the future, the proposed method should be tested on more data and compared with a log scaler classifying the timber. The log scaler estimates the number of annual rings and classifies the logs into quality classes using the number of annual rings as one of the classification parameters. To compare that result with classification using the proposed method would be an interesting evaluation, and can show if the proposed method is suitable as an automatic method or as a tool to help the log scaler in the estimation. Comparisons should also be made with the exact number of rings, computed in the correct direction according to the instructions given by the Swedish Timber Measurement Council.

Acknowledgement

Thanks to Anders Brun and Gunilla Borgefors, Centre for Image Analysis, Swedish University of Agricultural Sciences, for scientific discussions. The project is partly financed by the Swedish Timber Measurement Council, VMU.

References

1. He, Z., Munro, M.A.R., Gopalan, G., Kulkarni, V., Schowengerdt, R.A., Hughes, M.K.: System and algorithm design for a new generation tree-ring image analysis system. Optical Engineering 47(2) (2008)
2. Conner, W., Schowengerdt, R., Munro, M., Hughes, M.: Design of a computer vision based tree ring dating system. In: 1998 IEEE Southwest Symposium on Image Analysis and Interpretation, pp. 256–261 (1998)
3. Laggoune, H., Sarifuddin, G.V.: Tree ring analysis. In: Canadian Conference on Electrical and Computer Engineering, May 2005, pp. 1574–1577 (2005)
4. Soille, P., Misson, L.: Tree ring area measurements using morphological image analysis. Canadian Journal of Forest Research 31, 1074–1083 (2001)
5. Cerda, M., Hitschfeld-Kahler, N., Mery, D.: Robust tree-ring detection. In: Mery, D., Rueda, L. (eds.) PSIVT 2007. LNCS, vol. 4872, pp. 575–585. Springer, Heidelberg (2007)
6. Österberg, P., Ihalainen, H., Ritala, R.: Robust methods for determining quality properties of wood using digital log end images. In: The 12th Int. Conf. on Scanning Technology and Process Optimization in the Wood Industry, ScanTech. (2007)
7. Bayer, B.E.: Color imaging array, U.S. Patent No. 3,971,065 (1976)
8. The Swedish Timber Measurement Council: Regulations for measuring roundwood (1999)
9. Sonka, M., Hlavac, V., Boyle, R.: Image Processing, Analysis, and Machine Vision. Brooks/Cole Publishing Company (1999)
10. Norell, K., Borgefors, G.: Estimation of pith position in untreated log ends in sawmill environments. Computers and Electronics in Agriculture 63(2), 155–167 (2008)
11. Bigün, J., Granlund, G.H.: Optimal orientation detection of linear symmetry. In: Proceedings of the first international conference on computer vision, pp. 433–438. IEEE Computer Society Press, Los Alamitos (1987)
12. Yu, Z., Bajaj, C.: A fast and adaptive method for image contrast enhancement. In: Int. Conf. on Image Processing (ICIP), pp. 1001–1004 (2004)
13. Norell, K., Lindblad, J., Svensson, S.: Grey weighted polar distance transform for outlining circular and approximately circular objects. In: Int. Conf. on Image Analysis and Processing (ICIAP), pp. 647–652. IEEE Computer Society, Los Alamitos (2007)
14. Nain, D., Haker, S., Grimson, W.E.L., Cosman Jr., E.R., Wells III, W.M., Ji, H., Kikinis, R., Westin, C.-F.: Intra-patient prone to supine colon registration for synchronized virtual colonoscopy. In: Dohi, T., Kikinis, R. (eds.) MICCAI 2002. LNCS, vol. 2489, pp. 573–580. Springer, Heidelberg (2002)